HHS Public Access

Author manuscript

Neuroimage. Author manuscript; available in PMC 2019 April 15.

Published in final edited form as:

Neuroimage. 2018 April 15; 170: 307–320. doi:10.1016/j.neuroimage.2017.01.070.

Groupwise Structural Parcellation of the Whole Cortex: A Logistic Random Effects Model Based Approach

Guillermo Gallardo[a], **William Wells III**[b], **Rachid Deriche**[a], and **Demian Wassermann**[a]

[a]Université Côte d'Azur, Inria, France

[b]Harvard Medical School, Boston, Massachusetts, USA

Abstract

Current theories hold that brain function is highly related to long-range physical connections through axonal bundles, namely *extrinsic connectivity*. However, obtaining a groupwise cortical parcellation based on extrinsic connectivity remains challenging. Current parcellation methods are computationally expensive; need tuning of several parameters or rely on ad-hoc constraints. Furthermore, none of these methods present a model for the cortical extrinsic connectivity of the cortex. To tackle these problems, we propose a parsimonious model for the extrinsic connectivity and an efficient parceling technique based on clustering of tractograms. Our technique allows the creation of single subject and groupwise parcellations of the whole cortex. The parcellations obtained with our technique are in agreement with structural and functional parcellations in the literature. In particular, the motor and sensory cortex are subdivided in agreement with the human homunculus of Penfield. We illustrate this by comparing our resulting parcels with the motor strip mapping included in the Human Connectome Project data.

Keywords

Structural Parcellation; Statistical Clustering Models; Tractography; Structural Connectivity

1. Introduction

The human brain is arranged in areas based on criteria such as cytoarchitecture, functional specialization or axonal connectivity (Brodmann, 1909; Thirion et al., 2014; Thiebaut de Schotten et al., 2016). Parceling the cortex into such areas and characterizing their interaction is key to understanding how the brain works. Nowadays it is accepted that axonal connectivity plays a fundamental role in the interaction between brain regions (Schmahmann and Pandya, 2006). Moreover, current theories hold that long-range physical connections trough axonal bundles, namely *extrinsic connectivity*, are strongly related to brain function, for example, this has been shown in macaques (Passingham et al., 2002). Therefore, understanding how the cortex is arranged based on its extrinsic connectivity can provide key information in unraveling the internal organization of the brain.

Diffusion MRI (dMRI) enables the in vivo exploration of extrinsic connectivity and other aspects of white matter anatomy on the brain. However, in using diffusion MRI to infer long-distance connectivity, several challenges arise. A primary issue is the spatial resolution of diffusion imaging: it is several orders of magnitude coarser than axonal diameters (millimeters vs. micrometers) (Van Essen et al., 2014), making hard to infer some brain pathways. In addition, there is as yet no quantitative measure of the strength of connections from diffusion (Jbabdi and Behrens, 2013). Given these general limitations, obtaining a cortical parcellation based on extrinsic connectivity remains challenging (Van Essen et al., 2014; Jbabdi and Behrens, 2013). Moreover, most current parceling techniques compute either single-subject or groupwise parcellations. Single-subject techniques work by refining other parcellations (Clarkson et al., 2010), which introduces a bias in the resulting parcellation; parceling only part of the cortex (Lefranc et al., 2016; Roca et al., 2009; Thiebaut de Schotten et al., 2014, 2016) or using ad-hoc metrics to compare extrinsic connectivity (Moreno-Dominguez et al., 2014). Meanwhile, existing groupwise methods rely on average connectivity profiles (Clarkson et al., 2010; Roca et al., 2010), which prevents obtaining single subject parcellations; seek a matching across subjects after independent parcellations (Moreno-Dominguez et al., 2014), relying on possible noisy results, or need fine tuning of parameters, as the expected number of clusters to find (Parisot et al., 2015).

In this work, we present a parsimonious model for the cortical connectivity alongside an efficient parceling technique based on it. We summarize both contributions in Fig. 1. Our model assumes that the cortex is divided in patches of homogeneous extrinsic connectivity. That is, nearby neurons in the cortex share approximately the same long-range physical connections, we call this the *local coherence criterion*. Our assumption is based on histological results in the macaque brain (Schmahmann and Pandya, 2006). Inspired by statistical models for clustered data (Pendergast et al., 1996), our model accounts for the variability in the axonal connections of neurons within a patch and for variability in patch boundaries across subjects. Our parceling technique allows us to create single subject and groupwise parcellations of the whole cortex in agreement with extant parcellations.

We validate our technique by taking advantage of data available from the Human Connectome Project (HCP). Using our technique, we compute single subject and a groupwise parcellations. In this work we will focus on the groupwise case. For results of our method on the single-subject case please refer to Gallardo et al. (in press). Here, we first assess the consistency of our groupwise parceling technique by comparing the groupwise parcellations of three disjoint groups of 46 subjects from the HCP. We also show that our technique computes a similar parcellation to the one obtained by Thiebaut de Schotten et al. (2016) when parceling only the frontal cortex. Later, to test the functional specialization of our frontal lobe parcels, we use a data-base of meta-analysis of fMRI studies (Yarkoni et al., 2011), as in Thiebaut de Schotten et al. (2016). After, we show that our groupwise parcels subdivide some well-known anatomical structures by comparing our results against Desikan's atlas (Desikan et al., 2006). Also, we show the functional specialization of some of our parcels by comparing against results from Glasser et al. (2013). Finally, we compare our groupwise parcellation of 138 subjects against the multi-modal parcellation of Glasser et

al. (2016). We show that, while the parcellations boundaries differ, our parcels show similar or better functional specialization, specially for motor related tasks.

This work is organized as follows: In the Methods section we present our model for cortical connectivity and frame tractography within our model. Also, we present both our single-subject and groupwise case methodologies to parcellate the cortex. In the Experiments and Results section we present our results on HCP data. We then discuss our results and position ourselves with respect to the state of the art in the Discussion section. Finally, in the last section we provide our conclusions.

2. Methods

2.1. Cortical Connectivity Model and Tractography

Our model assumes that the cortex is divided in clusters of homogeneous extrinsic connectivity. That is, nearby neurons in the cortex share approximately the same long-ranged physical connections, we call this the *local coherence criterion*. Our assumption is based on histological results in the macaque brain (Schmahmann and Pandya, 2006). As in clustered data models in statistics (Pendergast et al., 1996), we allow intra-cluster and across-subject variability in the connectivity. We formalize this concept as:

$$K=\bigcup_{i=1}^{k} K_i, \forall_{1\leq i,j\leq k}, i \neq j \rightarrow K_i \cap K_j=\varnothing \wedge \mathrm{conn}(K_i) \neq \mathrm{conn}(K_j) \quad (1)$$

where the set of points on the cortex K is the disjoint union of each cluster K_i and conn(·) is the extrinsic connectivity fingerprint of a cluster. We will make the notion of variability explicit in eq. 3. In this work, the connectivity fingerprint of a seed-point in the brain is a binary vector denoting to which other seed-points it is connected through axonal bundles. That is, the physical connections of a point $p \in K_i$ in the brain are represented by its connectivity fingerprint conn(p) = conn(K_i).

Currently, the most common tool for estimating the extrinsic connectivity fingerprint of a point in vivo is probabilistic tractography (Jbabdi and Behrens, 2013). Given a seed-point in the brain, probabilistic tractography creates a *tractogram*: an image where each voxel is valued with its probability of being connected to the seed through axonal bundles. One way of calculating these probabilities is with a Monte Carlo procedure, simulating the random walk of water particles through the white matter (Behrens et al., 2003). Each one of these paths is known as a streamline. If we model these streamlines as Bernoulli trials, where we get a value for the connection from our seed with other points (1 if they connected by the streamline, 0 if not) (Behrens et al., 2003), then, we can model the tractogram of the subject s in the seed-point p as:

$$T_{sp}=[P(\tilde{C}_{spi}=1)]_{1\leq i\leq n}=[\theta_{spi}]_{1\leq i\leq n}, \quad \tilde{C}_{spi}\sim\mathrm{Bernoulli}(\theta_{spi}), \quad (2)$$

where $\tilde{C}_{spi}$ is a Bernoulli random variable[1] representing "the point p of the subject s is connected to the voxel i". Each Bernoulli's parameter (θ_{spi}) represents the probability of being connected, and is estimated as the proportion of success in the Bernoulli trials of each seed.

To formulate the tractogram in accordance to our hypothesis of cortical connectivity, we model it as a vector of random variables. In our model, each element in a tractogram comes from a random variable depending on the point's cluster along with its intra-cluster and across-subject variability:

$$p \in K_c \rightarrow \tilde{T}_{sp} = [P(\tilde{C}_{spi} = 1 | \mathrm{conn}(K_c), \tilde{\varepsilon}_{ci}, \tilde{\varepsilon}_{si})]_{1 \leq i \leq n}, \quad (3)$$

in this case, the point p belongs to the cluster c; $\tilde{\varepsilon}_{ci}$ represents the intra-cluster variability and $\tilde{\varepsilon}_{si}$ represents the across-subject variability for the connectivity to voxel i in the cluster c.

Since each $\tilde{C}_{spi}$ follows a Bernoulli distribution (Eq. 2) it is difficult to find an explicit formulation for $P(\tilde{C}_{spi} = 1/\mathrm{conn}(K_c), \tilde{\varepsilon}_{ci}, \tilde{\varepsilon}_{si})$ accounting for the variabilities. For this, we use the generalized linear model (GLM) theory. In this theory, the data is assumed to follow a linear form after being transformed with an appropriate link function (McCullagh and Nelder, 1989). Using the following notation abuse:

$$\mathrm{logit}(\tilde{T}_{sp}) \triangleq [\mathrm{logit}(P(\tilde{C}_{spi} = 1 | \mathrm{conn}(K_c), \tilde{\varepsilon}_{ci}, \tilde{\varepsilon}_{si})]_{1 \leq i \leq n}, \quad (4)$$

we derive from GLM a logistic random-effects model (Pendergast et al., 1996) for each point p:

$$\mathrm{logit}(\tilde{T}_{sp}) = \beta_c + \tilde{\varepsilon}_c + \tilde{\varepsilon}_s \in \mathbb{R}^n, \quad \tilde{\varepsilon}_c \sim \mathcal{N}(\overrightarrow{0}, \sigma_c^2 Id), \ \tilde{\varepsilon}_s \sim \mathcal{N}(\overrightarrow{0}, \sigma_s^2 Id), \quad (5)$$

where ε_c and ε_s represent the intra-cluster and across-subject variability respectively. According to GLM theory $\beta_c \in \mathbb{R}^n$ is the extrinsic connectivity fingerprint of cluster K_c transformed:

$$\mathrm{logit}^{-1}(\beta_c) = E(\tilde{T}_{sp}) = \mathrm{conn}(K_c). \quad (6)$$

The choice of logit as link function is based on the work of Pohl et al. (2007). In their work, Pohl et al. (2007) show that logit function's codomain is a Euclidean space, which allows us to transform and manipulate the tractograms in a well-known space.

[1]For the sake of clarity we denote all random variables with a tilde, e.g. $\tilde{C}$.

2.2. Single Subject and Groupwise Parceling Methodologies

In the previous section, we hypothesized that the cortex is divided in clusters with homogeneous extrinsic connectivity, alongside intra-cluster and across-subject variability. In using the previous hypothesis, it is important to remark that we don't have a priori knowledge of the cluster's location or their variability. But, thanks to the proposed logistic random effects model, we formulated the problem of finding these clusters as a well-known clustering problem. This is because, after transforming the tractograms with the logit function as in eq. 4 they will be in a Euclidean space (Pohl et al., 2007). Even more, eq. 5 states that the transformed tractograms come from a mixture of Gaussian distributions, e.g. it is a Gaussian mixture model.

To solve the Gaussian mixture model and find the clusters, we use a modified Agglomerative Hierarchical Clustering (AHC) algorithm. This was inspired by the method of Moreno-Dominguez et al. (2014). To enforce the local coherence criterion we also modify the algorithm to accept one parameter: the minimum size of the resulting clusters. Clusters smaller than this size are merged with neighbors, i.e. physically close clusters in the cortex. As we are working in a Euclidean space, we use Ward's Hierarchical Clustering method (Ward Jr., 1963). This method creates clusters with minimum within-cluster variance. The method's result is a dendrogram: a structure that comprises different levels of granularity for the same parcellation. This allows us to explore different parcellation granularities by choosing cutting criteria, without the need of recomputing each time.

The main advantage of the model we proposed in this work is that it allows us to create a groupwise parcellation using linear operations. Assuming direct seed correspondence across subjects, as in the HCP data set, our model lets us remove the subject variability of each seed's tractogram by calculating the expected value across subjects:

$$E_s(g(\tilde{T}_{sp}))=E_s(\beta_c+\tilde{\varepsilon}_c+\tilde{\varepsilon}_s),=\beta_c+\tilde{\varepsilon}_c+E_s\,(\tilde{\varepsilon}_s)=\beta_c+\tilde{\varepsilon}_c. \quad (7)$$

where the last equality is due to $E_s(\tilde{\varepsilon_s}) = 0$ (Eq. 5). Since in our model the variabilities are normally distributed (Eq. 5), we can estimate the expected value across subjects by averaging a seed's tractograms across subjects. This allows us to create population-representative tractograms for each seed free of across-subject variability, which then can be clustered to create a groupwise parcellation.

3. Experiments and Results

In the previous section we presented a model for the cortical extrinsic connectivity and a clustering technique to parcellate the whole brain. Our technique allows us to create single subject and groupwise parcellations, encoded with different levels of granularity in a dendrogram. Now, we show the results of applying our technique over the HCP dataset. First, we explain how the preprocessing step of tractography was made. Then, we elaborate in detail how we applied our technique. Later, we show that our groupwise technique creates results consistent when parceling different groups. Also, we show that our techniques creates parcels in accordance with those by Thiebaut de Schotten et al. (2016) when parceling only

the frontal lobe. Then, we present a proof-of-principle that our parcels are related to brain anatomy and functional specialization. Most of the results in this section are focused in the groupwise case, for further information on the single-subject technique please refer to Gallardo et al. (in press). Finally, we study the (dis)similarity between our groupwise parcellation and that of Glasser et al. (2016).

3.1. Data and Preprocessing

3.1.1. Human Connectome Project Dataset—A total of 138 subjects (65 males and 73 females, ages 31–35) were randomly selected from the group S500 of the Human Connectome Project (HCP). For information on the acquisition protocols please refer to Van Essen et al. (2012). Every subject has been already preprocessed with the HCP minimum pipeline (Glasser et al., 2013). Also, each subject's cortical surface is coregistered and represented as a triangular mesh of approximately 32000 vertices per hemisphere (Glasser et al., 2013). For each vertex, the corresponding label from Desikan's Atlas is known (Desikan et al., 2006). Finally, the group S500 contains tfMRI information representing the average response to functional stimuli in 100 unrelated subjects (U100)(Barch et al., 2013).

3.1.2. Probabilistic Tractography—To create the tractograms of each subject, we performed Constrained Spherical Deconvolution (CSD) based tractography (Tournier et al., 2004) from a dense set of points in the cortex. Specifically, since each subject has a mesh representing their gray-matter/white-matter interface (Glasser et al., 2013), we used their vertices as seeds to create tractograms. Vertices corresponding to the medial wall were excluded. To avoid superficial cortico-cortical fibers (Reveley et al., 2015), we shrank each of the 138 surfaces $2mm$ into the white matter. For each subject, we fitted a CSD model (Tournier et al., 2004) to their diffusion data using Dipy (version 0.11) (Garyfallidis et al., 2014) and created 5000 streamlines per seed-voxel using the implementation of probabilistic tractography in Dipy. Later, we created a tractogram as in (Eq. 2) by calculating for each seed the fraction of they particles that visited other seed-voxel.

3.2. Parceling Subjects From the Human Connectome Project

After performing tractography, we applied our parceling technique over each subject in our HCP sample. Specifically, we first transformed each tractogram with the logit function as in eq. 4. Then, we clustered the tractograms of each subject using the modified AHC algorithm while imposing a minimum cluster size of $3mm^2$ in the finest granularity. To retrieve parcellations from the resulting dendrogram we use the horizontal cut method (Murtagh and Contreras, 2011; Moreno-Dominguez et al., 2014; Gallardo et al., in press). Two examples of obtained single-subject parcellations at a granularity of 55 parcels are shown in fig. 2. To create the groupwise parcellation, we took advantage of the vertex correspondence across subjects in the HCP data set (Glasser et al., 2013). After transforming the tractograms with the logit transform, we computed the average connectivity of each seed by averaging its tractograms across-subject. Then, we computed the group-wise parcellation by clustering the averaged tractograms with our proposed technique (sec. 2.2). The obtained groupwise parcellation at a granularity of 55 parcels is shown in fig. 2.

3.3. Groupwise Parcellation Technique Consistency

To study the consistency of our technique, we randomly divided our HCP subject sample in 3 disjoint groups, trying to maintain the same proportion of males and females on each. The resulting groups had: 24 females, 22 males (group A); 23 females, 23 males (group B) and 28 females, 18 males (group C). For each group we computed their groupwise parcellation. The resulting parcellations at two different levels of granularity are shown in fig. 3.

To study the similarity between the obtained groupwise parcellations, we compared them at different levels of granularity using the adjusted Rand index (Hubert and Arabie, 1985). To have a baseline for the comparisons, we generated random parcellations of the cortex and computed the similarity between them. We computed two types of random parcellations: The first one is an homogeneous random parcellation with n parcels, inspired in a method used by Parisot et al. (2015). To compute it, we start by choosing n starting points in the cortex, then, we randomly expand each parcel on the cortex. By comparing these random parcellations between them we compute the minimum obtainable Rand index by mere chance at each level of granularity. In the second type of random parcellation, we simulate the behavior of our technique. For this, we create a parcellation with 300 parcels and then, we iteratively merge two parcels chosen at random until all the parcels are merged in one. By comparing these random parcellations between them we obtain the minimum obtainable Rand index by a random Hierarchical Clustering Algorithm. Examples of these random parcellations can be seen in Fig 4. The baselines presented in fig. 5 (yellow and violet lines) were computed by comparing 1000 of these random parcels at different levels of granularity.

The result of comparing the groupwise parcellations of each group appear in fig. 5. The figure shows that the similarity between our groupwise parcellations (lines red, green and blue) are significantly higher than the baselines (violet and yellow). That is, the similarity between our parcellations differs (for most cases) more than 3 standard deviations from the baselines' mean. Moreover, the similarity between our results differs more than 4 standard deviations from the comparison between synthetic hierarchical parcels. This results show that our groupwise parceling technique creates consistent parcellations.

3.4. Relationship with a Frontal Lobe Parcellation

Here we assess the agreement of our technique with an state-of-the-art extrinsic connectivity parceling technique. We do so by using our technique to parcellate the frontal lobe and compare our result against that of Thiebaut de Schotten et al. (2016). In their work, Thiebaut de Schotten et al. (2016) use a principal component analysis (PCA) statistical framework to parcellate the frontal lobe. They obtain a parcellation with 12 parcels. Then, they show that each one of these parcels possess a functional specialization by using the Decode tool[2] from Neurosynth (Yarkoni et al., 2011). Thiebaut's parcellation is currently available in Neurovault (Gorgolewski et al., 2016) as an annotated volume[3], registered on the Colin27 template (Holmes et al., 1996). We downloaded this parcellation and projected its parcels into a dense mesh representing the cortex of the Colin27 template. The dense mesh had the

[2] http://www.neurosynth.org/decode/
[3] http://neurovault.org/collections/1597/

same amount of vertices as our chosen HCP subjects, and such vertices were coregistered with the HCP subjects' cortical surfaces ones.

From the Desikan Atlas (Desikan et al., 2006) of each of our HCP subjects, we derived a groupwise mask for the frontal lobe. Then, we computed a groupwise parcellation with our technique, using only the tractograms in the mask. Figure 6 shows both the parcellation downloaded from Neurovault and our groupwise parcellation projected in the Colin template cortical surface. The figure shows our parcellation with 10 parcels since this level of granularity showed the best Rand index against the Thiebaut's parcellation. The colors of each parcel in our groupwise parcellation were picked in base to the position and amount of overlapping with the Thiebaut's parcels on the surface. While the similarity according to the Rand index is not significantly high (0.4), some visual similarity can be observed on the obtained parcellation, particularly in the blue, yellow, orange and green parcels. Moreover, as shown in table 1, our parcels show the same or even a higher level of functional specialization when processed with Neurosynth.

To study the consistency of our result we computed the frontal lobe groupwise parcellation in each of the 3 disjoint groups from the previous experiment. Figure 7 shows the three obtained parcellation alongside the Thiebaut's one. The obtained parcels show consistency, obtaining an adjusted Rand index score of 0.61 ± 0.05 between them. Finally, we studied if the masking affected the clustering of the frontal lobe. To do so, we applied the frontal lobe mask over a groupwise whole-brain parcellation of the 138 subjects. The resulting frontal lobe parcellation contained 12 parcels. This parcellation showed consistency with the one obtained by clustering only the tractograms in the frontal lobe. More specifically, the adjusted Rand index score between them was 0.65. We repeated this procedure for the 3 disjoints groups from the previous experiment. In each group, both frontal lobe parcellations showed to be consistent, achieving an adjusted Rand index of 0.57 ± 0.04.

3.5. Anatomical Relationship and Functional Specialization of Our Parcels

Here we present a proof of concept that our technique creates parcels within anatomical boundaries and with functional meaning. To do so, first, we extracted a parcellation with 55 parcels from the groupwise parcellation computed from the 138 subjects. This was made to get a parcellation with coarse granularity while having at least the amount of parcels in the anatomical atlas of Desikan (Desikan et al., 2006) (36 parcels). We compare this extracted parcellation against the Desikan Atlas and a functional study made to every subject in the HCP (Glasser et al., 2013).

3.5.1. Relationship with Anatomical Boundaries—To assess if some anatomical structures were present in the dendrogram and if our resulting parcels were subdividing them, we compared our extracted parcellation with the Desikan atlas (Desikan et al., 2006). To do so, we projected the Desikan regions over our parcels and then calculated: how many of our parcels were contained by a anatomical region in more than a 90%, and which anatomical regions were contained inside of one of our parcels. Using this criterion, the Insula; Cingulate; Lateral-Occipital; Fusiform; Superior Frontal; Lingual; Sensory and Motor Cortex appear to be found as shown in Fig. 8.

3.5.2. Functional Specialization—To study the relationship between our parcels and brain function, we projected our parcels over z-score maps representing responses to functional stimuli (Barch et al., 2013). These maps are available as part of the HCP data, and represent the average activation of 100 subjects. In particular, we used the maps related to the following tasks: right hand, foot and tongue movement; face, shape recognition and story categorization. For information on the functional tasks, acquisition and processing of this data please refer to Barch et al. (2013). Figure 9 shows our parcels projected over contrasts in motor tasks. In particular, our parcels are projected over the following contrasts: tongue-average; hand movement-average and foot movement-average. Figure 10 shows our parcels projected over contrasts in cognitive tasks: face-shape recognition; shape-face recognition and short-story categorization. The figures show a good overlap between our parcels and the regions with maximum activation of each task. In both figures the distribution of z-scores inside of specific regions are shown as histograms. Further information about the z-score is present in tables 2 and 3. These tables show that our parcels contain zero or few negatives values; that the mean of their contained z-score is always positive and also, that many of those parcels enclose the maximum achievable z-score.

3.6. Relationship with a Multi-Modal Parcellation of the Cortex

Finally, we study the (dis)similarities between our groupwise parcellation and that of Glasser et al. (2016). In their work, Glasser et al. (2016) compute a parcellation of the whole cortex using information from different MRI modalities. In particular, they use information from task functional MRI; resting state functional MRI; myelin maps computed from T1 and T2 images and cortical thickness. It is important to remark that dMRI data, in which our work is solely based, was not used to construct their parcellation.

To compare our results against Glasser's atlas, we first extracted a parcellation of 180 parcels from the groupwise dendrogram of our 138 HCP subjects. That is, we extracted a parcellation with the same number of parcels as Glasser's one. Figure 11 show both parcellations side by side. We compared both parcellations using the adjusted Rand Index, obtaining a score of 0.28. Such low score indicates that there's almost no similarity between our result and that of Glasser et al. (2016). Also, there's no relationship with our groupwise parcellation with 55 parcels used in the previous section since Glasser's parcels (finest) do not subdivide ours (coarsest). Since Glasser's parcellation comes from functional information in the HCP, we studied the functional specialization of its parcels in the same manner as previous section. Figure 12 shows the histogram of z-score contained for some parcels when using the same maps as in section Functional Activations. It's important to remark that the z-score maps used come from responses to functional stimuli of HCP subjects (Glasser et al., 2013). In particular, histograms a; b and c in fig. 12 show that their subdivisions of the sensorimotor cortex contain a wide range of z-scores, centered in zero.

4. Discussion

In this work we presented a parsimonious statistical model for long-ranged axonal connectivity. Our model (section 2.1), assumes that the cortex is divided in patches of homogeneous extrinsic connectivity, as histological results showed in the macaque brain

(Schmahmann and Pandya, 2006). By borrowing ideas from statistical clustered data models (Pendergast et al., 1996), our model accounts for the variability in the axonal connections of a patch's neurons and for variability in patch boundaries across subjects.

Taking advantage of our proposed model, in Section 2.2 we presented an efficient technique to parcellate the cortex based on its extrinsic connectivity. Our technique uses only dMRI information, without the need of relying on initial parcellations (Clarkson et al., 2010). Also, our technique allows parcellation of the whole cortex, overcoming the problem of working with only part of it (Lefranc et al., 2016; Roca et al., 2009; Thiebaut de Schotten et al., 2014, 2016). Additionally, our technique allows creation of both single subject and groupwise parcellations. Our groupwise parcellation technique relies on anatomical seed-correspondence across subjects. In our experiments, this is achieved as each HCP subject possess a coregistered dense mesh representing they cortical surface (Glasser et al., 2013). Given the anatomical differences across-subjects, this purely anatomical matching of seeds is probably sub-optimal. However, it allows us to compute single and groupwise parcellations independently. By doing this, we avoid the need to impose constraints between our single and group parcellations (Clarkson et al., 2010; Roca et al., 2010; Parisot et al., 2015).

Inspired by Moreno-Dominguez et al. (2014), our technique uses Hierarchical Clustering to comprise multiple granularities of the same parcellation in a dendrogram. This allows us to overcome the need of other techniques (Parisot et al., 2015) to specify an expected number of clusters. Hence, we don't need to recompute the whole pipeline each time a new parcellation is required. As in Moreno-Dominguez et al. (2014), we also create the dendrogram using only one comprehensive parameter: the minimum size of each cluster. This parameter imposes the local coherence criterion. Our fundamental difference with Moreno-Dominguez' technique is how we compare and merge tractograms during the clustering process. Moreno-Dominguez et al. (2014) use Centroid Clustering (Murtagh, 1985) with the cosine distance. This can lead to an erroneous parcellation since the centroid criterion doesn't minimize the cosine distance between points. Also, their method creates dendrograms with inversions (Murtagh, 1985), which are then removed heuristically. In our case, using a Logistic Random Effect model (eq. 5) allowed us to transform the tractograms into a Euclidean space (sec. 2.2) and compare them using the Euclidean distance. In doing this, it is important to remark that we are making a trade off. Since we are comparing high-dimensional vectors with the Euclidean distance, we are probably affected by the dimensionality curse (Beyer et al., 1999). However, working in an Euclidean space possess many advantages. The first advantage is that we can compute clusters with minimum intra-cluster variance by using Ward's Hierarchical method. We can use this algorithm since its only hypothesis is that the features to cluster are in a Euclidean space. Also, since we work with the Euclidean distance, we can apply the Lance and Williams (Lance and Williams, 1967) formula during clustering. This formula gives us the dissimilarity between the new centroid created at each step and the rest of the existing tractograms in constant time. As far as we know there's no Lance and Williams formula when using the cosine distance with the centroid linkage. This allows us to lower the time complexity of our algorithm with respect to Moreno-Dominguez. Since we use Ward's clustering, our resulting dendrograms do not have inversions, which means that we don't need to postprocess them. Another advantage is

that we can retrieve a parcellation from the dendrogram using a simple technique: horizontal cut (Murtagh and Contreras, 2011). While other methods to cut the dendrogram exist (Murtagh and Contreras, 2011), horizontal cut is sufficient to solve our Gaussian Mixture Model (eq. 5) as shown in Gallardo et al. (in press). Finally, even if our algorithm is probably affected by the dimensionality curse, our parcellations showed to be consistent across-groups and in agreement with extant parcellations in the literature.

4.1. Our Groupwise Parcellations are Consistent Across Similar Groups

We assessed the consistency of our groupwise parcellation by quantifying the consistency across 3 disjoint groups of 46 subjects each. The consistency is shown by the adjusted Rand index in Fig. 5, which quantifies consistency across parcellations (Hubert and Arabie, 1985). As seen in Fig. 5 whole-cortex parcellations obtained with our method are consistent across groups, and the Adjusted Rand Index is significantly higher, i.e. more than 3 standard deviations, for all granularities when compared with the null case of randomly-generated parcellations.

Our whole-cortex groupwise parcellation reaches a maximum consistency score when the cortex is divided in 6 regions, see Fig. 5. As seen in Fig. 3, these parcellations are consistent with specific anatomo/functional networks: the frontal lobe section anterior to the prefrontal cortex is shown in yellow; the sensorimotor area is shown in cyan, the cingulate area is shown in beige; the fronto-occipital connection in orange, and the temporo-parietal system in pink.

4.2. Our Method Creates Parcels in Agreement With a Single-Lobe Parceling Technique Extant in the Literature

We showed that our technique obtains results similar to another method extant in the literature. We did so by parceling only the frontal and showing the visual similarity between our resulting parcels and those obtained by Thiebaut de Schotten et al. (2016). Moreover, the blue, pink and green parcels in fig. 6 share not only similar boundaries and location, but also functional specialization (Table 1). In some cases our parcels possess even higher spatial-correlation with functional task according to Neurosynth's (Yarkoni et al., 2011) Decode tool[4]. We assessed the consistency of our obtained groupwise parcellation by computing the groupwise frontal lobe parcellation of three disjoints groups of 46 subjects and comparing them using the adjusted Rand index. The obtained value of 0.61 shows that our parcellation of the frontal lobe is consistent across groups.

4.3. Our Method Creates Several Parcels in Agreement with Brain Anatomy

We showed that many of our parcels are in agreement with brain anatomy. In particular, we showed that in our groupwise parcellation, with 55 parcels, the following anatomical structures appeared to be found: Cingulate; Insula; Lateral-Occipital; Fusiform; Superior Frontal; Lingual; Motor and Sensory cortex. Here we discuss why some of these parcels were found and how are their conectivity fingerprints. In the case of the Cingulate, its fingerprint, shown in fig. 13, is strongly related with the Cingulate Fascicle (CF) pathway.

[4] http://neurosynth.org/decode/

This is consistent with the fact that the seeds located in the Cingulate will end up into the CF after being pushed in the white-matter. In the case of the Insula, each subdivision showed a specific pattern of connectivity as shown in fig. 13. These parcels show a gradient of connections from the occipital lobe to the frontal lobe consistent with that of Ghaziri et al. (2015). In the Lateral-Occipital region, we see a specific pattern of local connectivity which cannot be attributed to gyral bias since the Lateral-Occipital covers many sulci and gyrus. In the case of the fusiform, it is almost completely contained in one of our parcellations, which goes from the Fusiform up to the Lateral-Occipital (fig. 8). This could add evidence to the hypothesis that the Fusiform plays a role in visual tasks (Kanwisher and Yovel, 2006; Yeatman et al., 2014). Finally, the Motor and Sensory cortex appear to be found. While the appearance of each gyri is most probably because of gyral bias (Van Essen et al., 2014), the parcels inside them show specific patterns of structural connectivity (fig. 13), and, as seen in section 3.5.2, functional specialization.

4.4. Our Results Show a Close Relationship Between Structural Connectivity and Brain Function

We assessed the functional specialization of some of our parcels by showing how they overlap with responses to functional and cognitive tasks measured with fMRI. In particular, for all the studied tasks, the parcels contained a higher proportion of positive values than negative ones as expressed by the positive mean values reported in tables 2 and 3. For some parcels there were not even negative values. Moreover, several of the histograms on figures 9 and 10 show a high frequency of z-score values greater than 5, which indicate a significant correlation with functional activation. Therefore, our results show, for some tasks, the strong relationship between extrinsic connectivity and functional specialization in the human brain cortex.

4.5. Our Parcels Are Not Similar to Those Obtained by Glasser et al. (2016) But Possess Better Functional Specialization for Motor Tasks

Our parcels were not related to those of Glasser et al. (2016). This is shown by the obtained adjusted Rand index score between them (0.28). It’s important to remark that our parcels are purely based on extrinsic connectivity, meanwhile those of Glasser et al. (2016) do not use dMRI information. Glasser’s parcels are mostly based on myelin and functional information. In particular, their subdivision of the sensori-motor cortex (green parcels in fig. 11) is mostly based in Myelin maps as shown in Figure 4.a of Glasser et al. (2016). Because of this, their parcels in the sensori-motor cortex contain a wide range of z-scores when compared with responses to functional stimuli as shown by histograms a; b and c in fig. 12. In contrast, our parcels in the sensori-motor cortex, for a coarser parcellation, show a good overlap with function and are in agreement with the motor strip mapping as discussed in the previous section. Also, for the case of story categorization; shape recognition and face recognition, our parcels show a similar distribution of z-scores (fig. 9) than those with the highest mean z-scores of Glasser et al. (2016) (parcels d; e and f of fig. 12).

5. Conclusion

Understanding how the brain is structurally organized and its relationship with functionality is an open question in neuroscience. Recent advances in acquisition and modeling techniques on dMRI have facilitated to study axonal connectivity in the brain. However, parceling the whole cortex based on a structural criterion remained challenging. In this work we presented a connectivity model; framed tractography within our model and presented a parceling technique that allows parcellation of the whole brain in both single subject and groupwise cases. Our technique, along with the obtained groupwise parcellation, could have major implications both in cognitive neuroscience and in development-aging studies. At the same time, our technique could help to lower the gap between structural connectivity and brain function, since some of our pure structural parcels showed good overlapping with responses to functional tasks.

Both our parceling tool and the obtained groupwise parcellation are or will be soon freely available in GitHub (https://github.com/AthenaEPI/logpar) and Neurovault. These tools provide a sound basis for new studies on human cognition, brain development, aging and disease. These tools can create fine parcellations of cortical areas, improving our knowledge about cortical organization. Future comparison with functional connectivity could lead to finally unraveling the link between axonal connectivity and brain function.

Acknowledgments

This work has received funding from the European Research Council (ERC) under the European Union's Horizon 2020 research and innovation program (ERC Advanced Grant agreement No 694665: CoBCoM). This work has received funding from the Inria Associated Team Large Brain Nets Grant. This work also has received the following funding: NIH P41EB015902.

References

Barch DM, Burgess GC, Harms MP, Petersen SE, Schlaggar BL, Corbetta M, Glasser MF, Curtiss S, Dixit S, Feldt C, Nolan D, Bryant E, Hartley T, Footer O, Bjork JM, Poldrack R, Smith S, Johansen-Berg H, Snyder AZ, Van Essen DC. Function in the human connectome: Task-fMRI and individual differences in behavior. Neuroimage. Oct.2013 80:169–189. [PubMed: 23684877]

Behrens T, Woolrich M, Jenkinson M, Johansen-Berg H, Nunes R, Clare S, Matthews P, Brady J, Smith S. Characterization and propagation of uncertainty in diffusion-weighted MR imaging. Magn Reson Med. Nov; 2003 50(5):1077–1088. [PubMed: 14587019]

Beyer K, Goldstein J, Ramakrishnan R, Shaft U. When is "nearest neighbor" meaningful? Database Theory—ICDT'99. 1999:217–235.

Brodmann, K. Vergleichende Lokalisationslehre der Groβhirnrinde in ihren Prinzipien dargestellt aufGrund des Zellaufbaues. Leipzig: Barth; 1909.

Clarkson, MJ., Malone, IB., Modat, M., Leung, KK., Ryan, N., Alexander, DC., Fox, NC., Ourselin, S. Vol. 6362 of Lecture Notes in Computer Science. Springer Berlin Heidelberg; Berlin, Heidelberg: 2010. A Framework For Using Diffusion Weighted Imaging To Improve Cortical Parcellation.

Desikan RS, Ségonne F, Fischl B, Quinn BT, Dickerson BC, Blacker D, Buckner RL, Dale AM, Maguire RP, Hyman BT, Albert MS, Killiany RJ. An automated labeling system for subdividing the human cerebral cortex on MRI scans into gyral based regions of interest. Neuroimage. Jul; 2006 31(3):968–980. [PubMed: 16530430]

Gallardo, G., Fick, R., Wells, WI., Deriche, R., Wassermann, D. MICCAI 2016 Work Comput Diffus MRI. Springer International Publishing; Groupwise Structural Parcellation of the Cortex: A Sound Approach Based on Logistic Models. in pressURL https://hal.archives-ouvertes.fr/hal-01358436

Garyfallidis E, Brett M, Amirbekian B, Rokem A, van der Walt S, Descoteaux M, Nimmo-Smith I. Dipy, a library for the analysis of diffusion MRI data. Front Neuroinform. Feb.2014 :8. [PubMed: 24600385]

Ghaziri J, Tucholka A, Girard G, Houde J-C, Boucher O, Gilbert G, Descoteaux M, Lippe S, Rainville P, Nguyen DK. The Corticocortical Structural Connectivity of the Human Insula. Cereb Cortex. 2015:1–13. [PubMed: 23926113]

Glasser MF, Coalson TS, Robinson EC, Hacker CD, Harwell J, Yacoub E, Ugurbil K, Andersson J, Beckmann CF, Jenkinson M, Smith SM, Van Essen DC. A multi-modal parcellation of human cerebral cortex. Nature. 2016; 536(7615):171–8. [PubMed: 27437579]

Glasser MF, Sotiropoulos SN, Wilson JA, Coalson TS, Fischl B, Andersson JL, Xu J, Jbabdi S, Webster M, Polimeni JR, Van Essen DC, Jenkinson M. The minimal preprocessing pipelines for the Human Connectome Project. Neuroimage. Oct.2013 80:105–124. [PubMed: 23668970]

Gorgolewski KJ, Varoquaux G, Rivera G, Schwartz Y, Sochat VV, Ghosh SS, Maumet C, Nichols TE, Poline JB, Yarkoni T, Margulies DS, Poldrack RA. NeuroVault.org: A repository for sharing unthresholded statistical maps, parcellations, and atlases of the human brain. Neuroimage. 2016; 124(April):1242–1244. [PubMed: 25869863]

Holmes CJ, Hoge R, Collins L, Evans AC. Enhancement of T1 MR images using registration for signal averaging. Neuroimage. Jun.1996 3(3):S28.

Hubert L, Arabie P. Comparing partitions. J Classif. Dec; 1985 2(1):193–218.

Jbabdi S, Behrens TE. Long-range connectomics. Ann N Y Acad Sci. Dec; 2013 1305(1):83–93. [PubMed: 24329486]

Kanwisher N, Yovel G. The fusiform face area: a cortical region specialized for the perception of faces. Philos Trans R Soc Lond B Biol Sci. 2006; 361(1476):2109–28. [PubMed: 17118927]

Lance BGN, Williams WT. A general theory of classificatory sorting strategies 1. Hierarchical systems. Comput J. 1967; 9(4):373–380.

Lefranc S, Roca P, Perrot M, Poupon C, Le Bihan D, Mangin J-F, Rivière D. Groupwise connectivity-based parcellation of the whole human cortical surface using watershed-driven dimension reduction. Med Image Anal. May.2016 30:11–29. [PubMed: 26849421]

McCullagh, P., Nelder, JA. Generalized Linear Models. 2. Chapman and Hall/CRC; 1989.

Moreno-Dominguez D, Anwander A, Knösche TR. A hierarchical method for whole-brain connectivity-based parcellation. Hum Brain Mapp. Oct; 2014 35(10):5000–5025. [PubMed: 24740833]

Murtagh, F. Multidimensional Clustering Algorithms. Comps Physica Verlag; Vienna: 1985.

Murtagh F, Contreras P. Methods of Hierarchical Clustering. Empir Econ. Apr; 2011 38(1):23–45.

Parisot S, Arslan S, Passerat-Palmbach J, Wells WM, Rueckert D. Tractography-Driven Groupwise Multi-scale Parcellation of the Cortex. Inf Process Med Imaging. 2015; 24:600–12. [PubMed: 26221706]

Passingham RE, Stephan KE, Kötter R. The anatomical basis of functional localization in the cortex. Nat Rev Neurosci. Aug; 2002 3(8):606–616. [PubMed: 12154362]

Pendergast JF, Gange SJ, Newton MA, Lindstrom MJ, Palta M, Fisher MR. A Survey of Methods for Analyzing Clustered Binary Response Data. Int Stat Rev/Rev Int Stat. Apr.1996 64(1):89.

Pohl KM, Fisher J, Bouix S, Shenton M, McCarley RW, Grimson WEL, Kikinis R, Wells WM. Using the logarithm of odds to define a vector space on probabilistic atlases. Med Image Anal. Oct; 2007 11(5):465–477. [PubMed: 17698403]

Reveley C, Seth AK, Pierpaoli C, Silva AC, Yu D, Saunders RC, Leopold Da, Ye FQ. Superficial white matter fiber systems impede detection of long-range cortical connections in diffusion MR tractography. Proc Natl Acad Sci. May; 2015 112(21):E2820–E2828. [PubMed: 25964365]

Roca P, Rivière D, Guevara P, Poupon C, Mangin JF. Tractography-based parcellation of the cortex using a spatially-informed dimension reduction of the connectivity matrix. Lect Notes Comput Sci (including Subser Lect Notes Artif Intell Lect Notes Bioinformatics) 5761 LNCS (PART 1). 2009:935–942.

Roca P, Tucholka A, Rivière D, Guevara P, Poupon C, Mangin JF. Inter-subject connectivity-based parcellation of a patch of cerebral cortex. Lect Notes Comput Sci (including Subser Lect Notes Artif Intell Lect Notes Bioinformatics) 6362 LNCS (PART 2). 2010:347–354.

Schmahmann, JD., Pandya, DN. Fiber Pathways of the Brain. Vol. 1. Oxford University Press; Apr. 2006

Thiebaut de Schotten M, Urbanski M, Batrancourt B, Levy R, Dubois B, Cerliani L, Volle E. Rostro-caudal Architecture of the Frontal Lobes in Humans. Cereb Cortex. 2016:1–15. [PubMed: 25139941]

Thiebaut de Schotten M, Urbanski M, Valabregue R, Bayle DJ, Volle E. Subdivision of the occipital lobes: An anatomical and functional MRI connectivity study. Cortex. 2014; 56:121–137. [PubMed: 23312799]

Thirion B, Varoquaux G, Dohmatob E, Poline JB. Which fMRI clustering gives good brain parcellations? Front. Neurosci. 2014; 8(8 JUL):1–13.

Tournier JD, Calamante F, Gadian DG, Connelly A. Direct estimation of the fiber orientation density function from diffusion-weighted MRI data using spherical deconvolution. Neuroimage. Nov; 2004 23(3):1176–1185. [PubMed: 15528117]

Van Essen, DC., Jbabdi, S., Sotiropoulos, SN., Chen, C., Dikranian, K., Coalson, T., Harwell, J., Behrens, TE., Glasser, MF. Diffus MRI No January 2014. Elsevier; 2014. Mapping Connections in Humans and Non-Human Primates; p. 337-358.

Van Essen DC, Ugurbil K, Auerbach E, Barch D, Behrens TEJ, Bucholz R, Chang A, Chen L, Corbetta M, Curtiss SW, Della Penna S, Feinberg D, Glasser MF, Harel N, Heath aC, Larson-Prior L, Marcus D, Michalareas G, Moeller S, Oostenveld R, Petersen SE, Prior F, Schlaggar BL, Smith SM, Snyder aZ, Xu J, Yacoub E. The Human Connectome Project: A data acquisition perspective. Neuroimage. 2012; 62(4):2222–2231. [PubMed: 22366334]

Ward J Jr. Hierarchical Grouping to Optimize an Objective Function. J Am Stat Assoc. 1963; 58(301): 236–244.

Yarkoni T, Poldrack RA, Nichols TE, Van Essen DC, Wager TD. Large-scale automated synthesis of human functional neuroimaging data. Nat Methods. Jun; 2011 8(8):665–670. [PubMed: 21706013]

Yeatman JD, Weiner KS, Pestilli F, Rokem A, Mezer A, Wandell BA. The vertical occipital fasciculus: A century of controversy resolved by in vivo measurements. Proc Natl Acad Sci. Dec; 2014 111(48):E5214–E5223. [PubMed: 25404310]

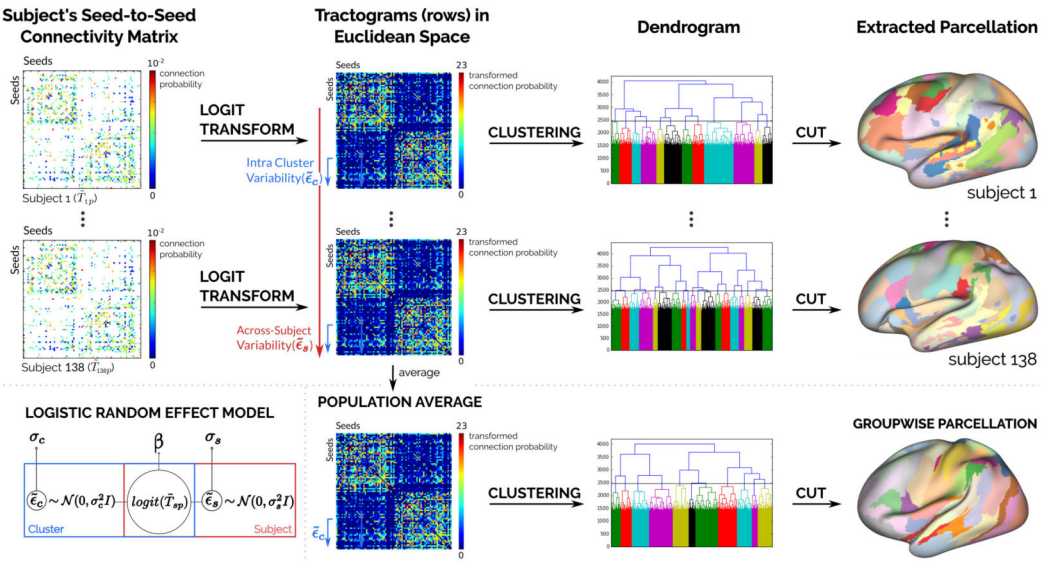

Figure 1.

Lower left corner: graphical model of the linear relationship between the tractogram of a subject s for a seed p ($\tilde{T}_{sp}$); and the intra-cluster ($\tilde{\varepsilon}_C$) and across-subject ($\tilde{\varepsilon}_S$) variability of the seed's patch. We transform the tractograms into a Euclidean space while explicitly accounting for the variability. This allows us to use well known clustering techniques and compress different levels of granularities for a same parcellation in a dendrogram.

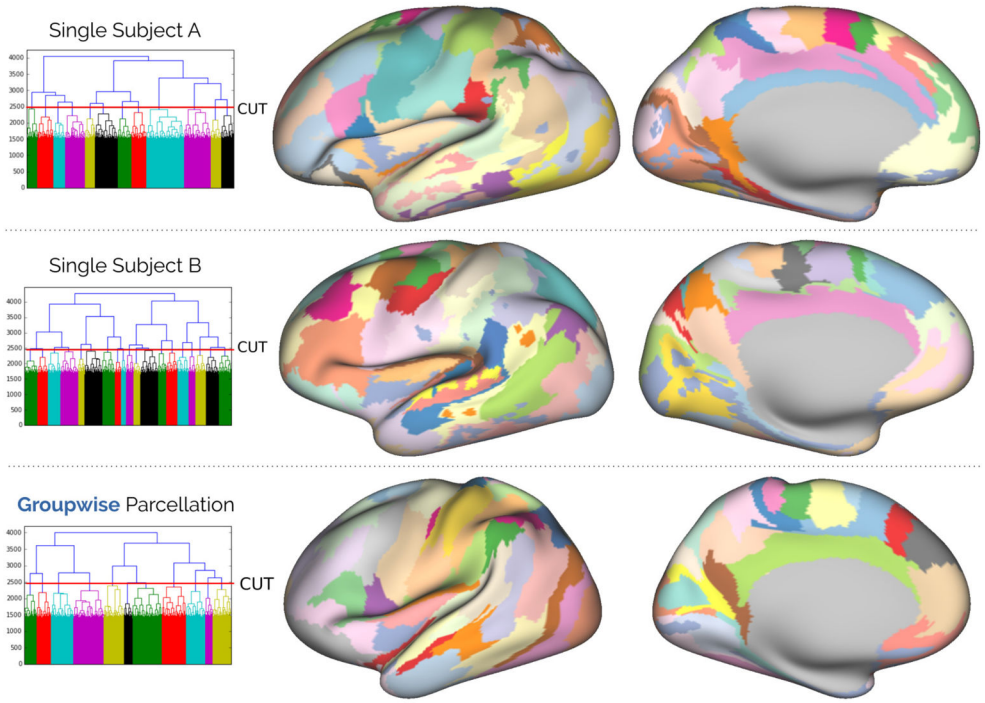

Figure 2.

Examples of two single-subject parcellations and the groupwise parcellations computed with our technique. All the parcellations shown have 55 parcels. The corresponding dendrogram for each case, along with the chosen cut height (red line) are shown. The groupwise parcellation is based on 138 subjects from the Human Connectome Project.

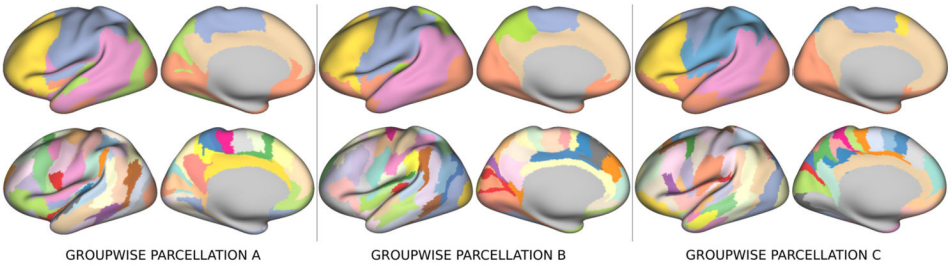

Figure 3.

Groupwise parcellations of 3 disjoint groups of 46 people each. We show results from the same dendrogram cut to get 6 parcels (upper) and 55 parcels (lower). Labels with best overlap in upper figures share the same color. Notice that there are two different shades of blue for the group C.

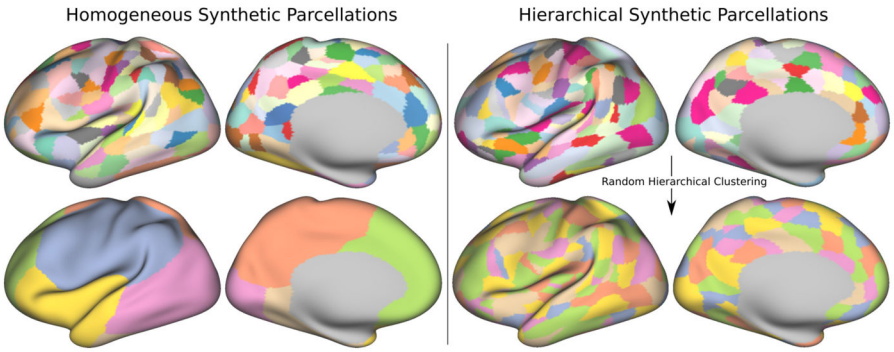

Figure 4.

Examples of synthetic parcellations created to compute a baseline adjusted rand index. Parcellations on the left were created by dividing the brain in a homogeneous way, inspired by the random parcellation presented in Parisot et al. (2015). Parcellations on the right were created by randomly merging parcels of a coarse parcellation.

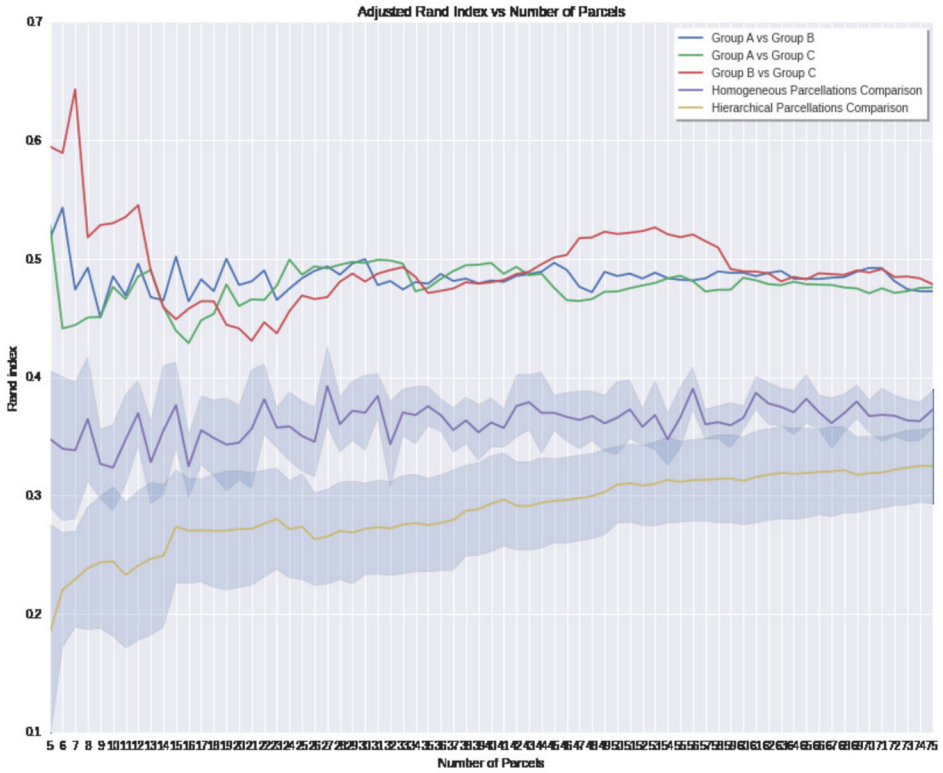

Figure 5.

Adjusted Rand Index obtained when comparing: (red) Group A vs Group B; (blue) Group A vs Group C; (green) Group B vs Group C; (purple) Synthetic Homogeneous Parcels and (yellow) Synthetic hierarchical Parcels.

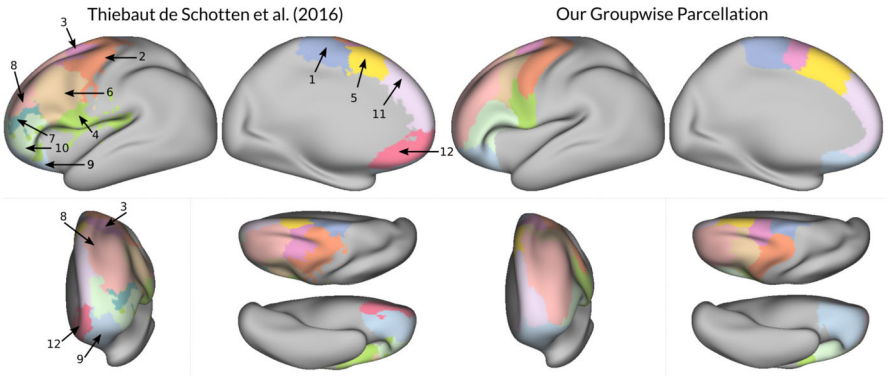

Figure 6.

Thiebaut de Schotten et al. (2016) parcellation (left) and our groupwise parcellation using only tractograms from the frontal lobe (right). Our parcels are colored after the parcel from Thiebaut de Schotten et al. (2016) with which they best overlap.

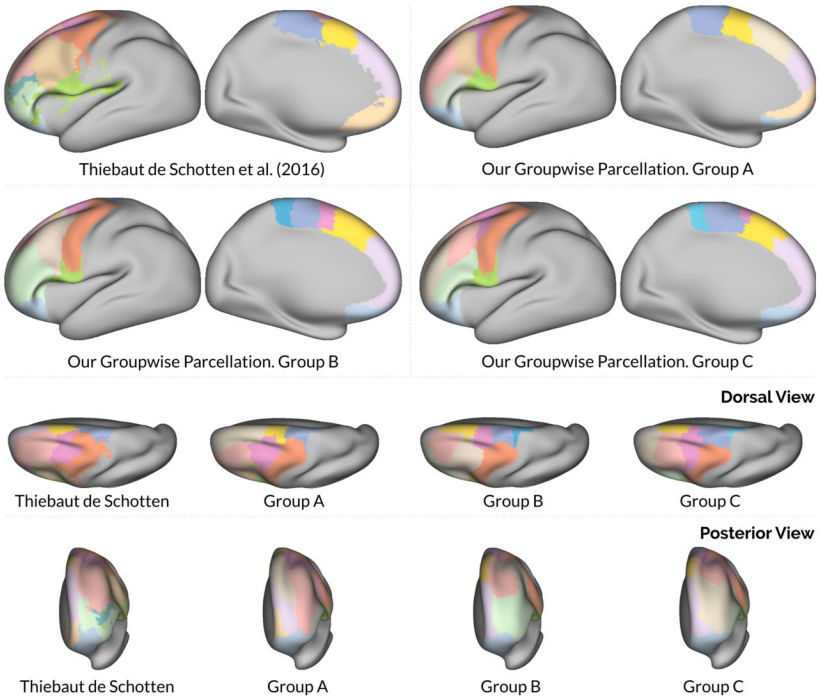

Figure 7.

Thiebaut de Schotten et al. (2016) parcellation (top-left) and our frontal lobe groupwise parcellations computed over 3 disjoint groups of subjects. Our parcels are colored after the parcel from Thiebaut de Schotten et al. (2016) with which they best overlap.

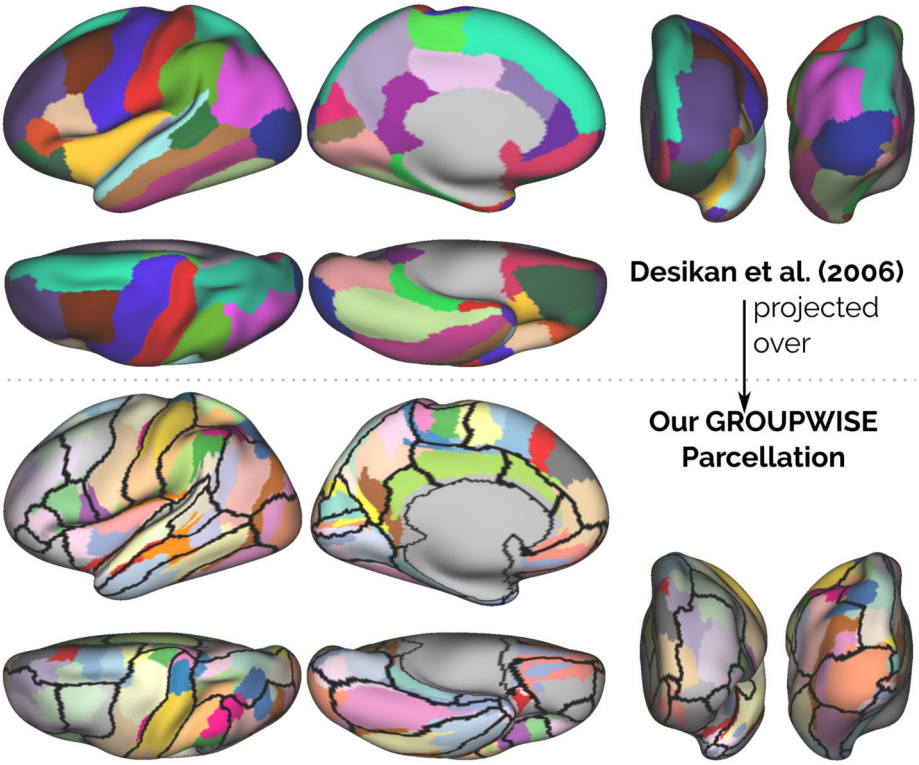

Figure 8.

Relation between our pure extrinsic parcellation and the anatomical atlas of Desikan (Desikan et al., 2006). Desikan atlas projected over the groupwise parcellation with 55 parcels. Insula; Cingulate; Lateral-Occipital; Fusiform; Superior Frontal; Lingual; Sensory and Motor Cortex appear to be found.

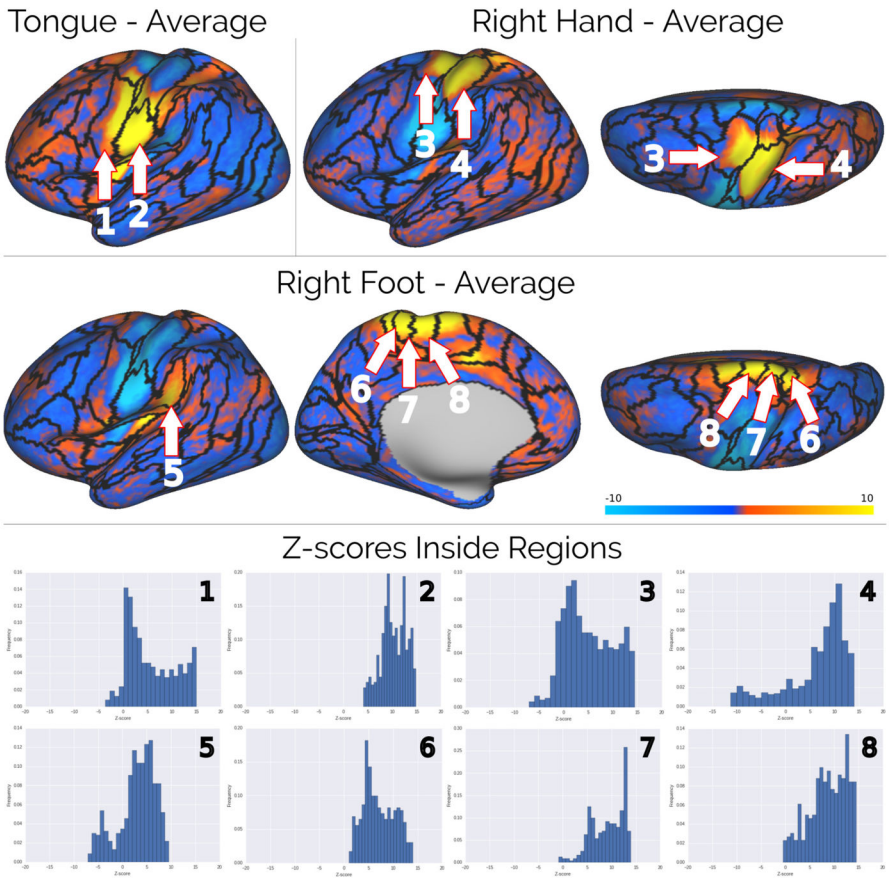

Figure 9.

Our groupwise parcellation with 55 parcels projected over z-scores representing responses to motor tasks. Each histogram shows the distribution of z-score inside our parcels. The null or small fraction of negative values shows the functional specialization of our parcels

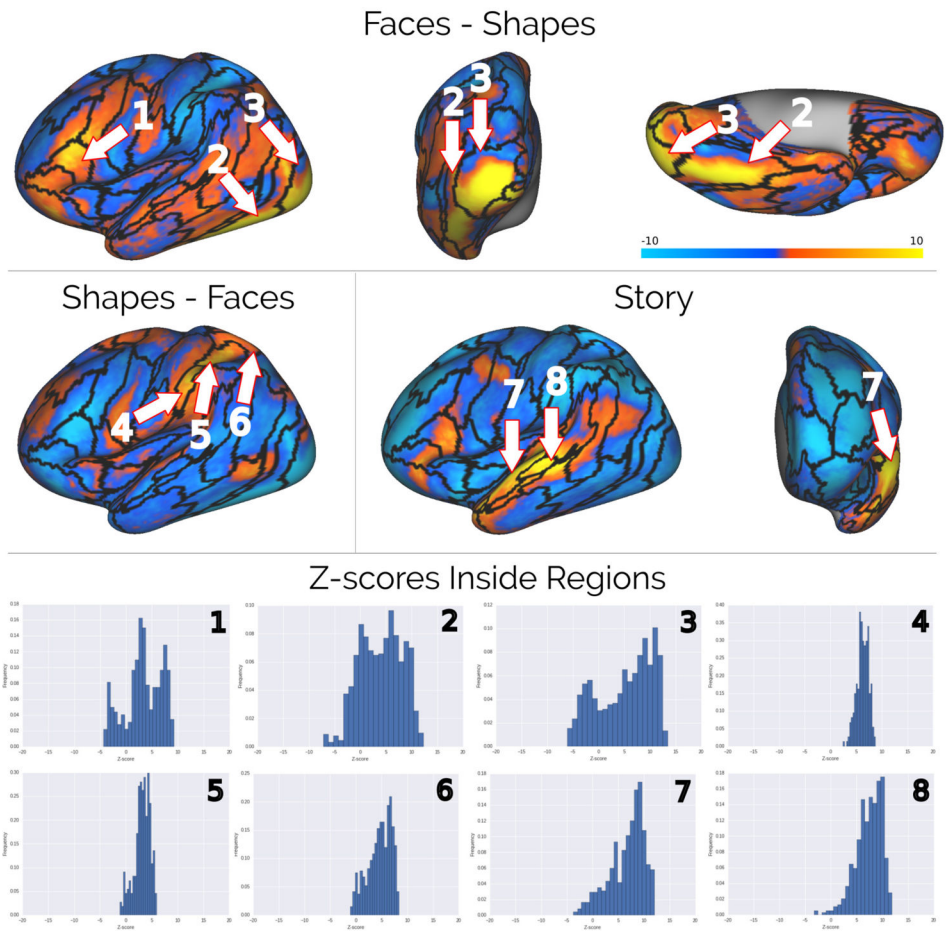

Figure 10.

Our groupwise parcellation with 55 parcels projected over z-scores representing responses to cognitive tasks. Each histogram shows the distribution of z-score inside our parcels. The null or small fraction of negative values shows the functional specialization of our parcels

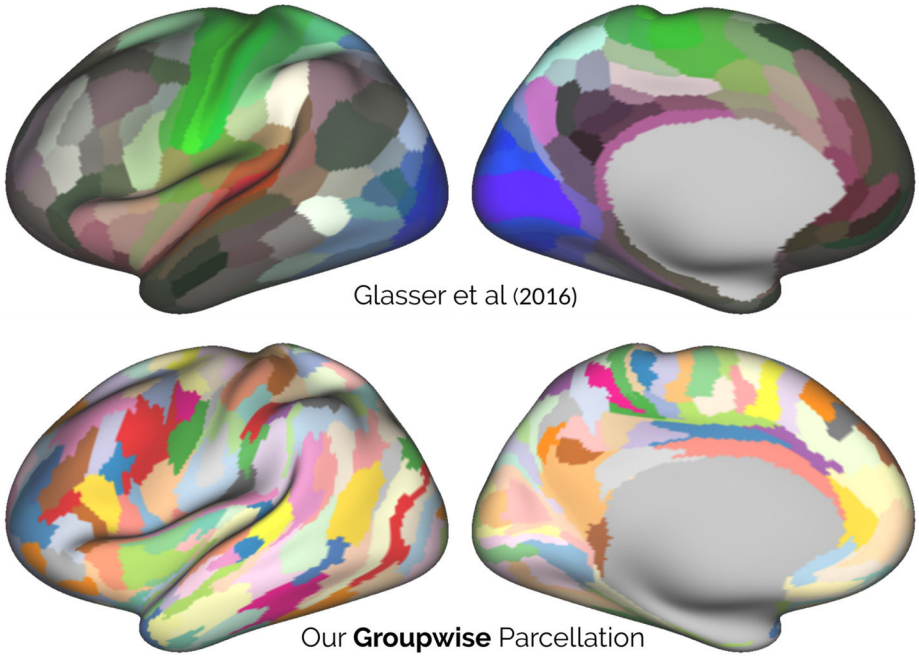

Figure 11.

Glasser et al. (2016) parcellation (upper) and our groupwise parcellations computed from 138 HCP subjects. Both parcellations contain 180 parcels. There's almost no overlap according to the adjusted Rand index between them (0.28).

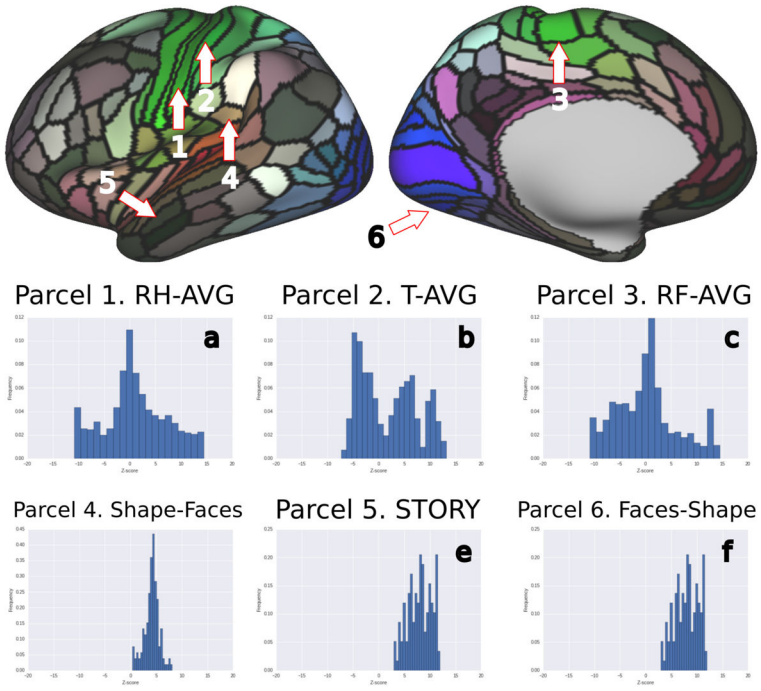

Figure 12.

Glasser et al. (2016) parcellation (upper) and histograms of z-score contained in different parcels for different functional task. (a) Histogram for parcel 1 for the contrast related to Tongue movement. (b) Histogram for parcel 2 for the contrast related to Tongue movement. (c) Histogram for parcel 3 for the contrast related to Right Foot movement. (d) Histogram for parcel 4 for the contrast Shape recognition vs Face recognition. (e) Histogram for parcel 5 for the contrast related to Story Categorization. (f) Histogram for parcel 5 for the contrast Face recognition vs Shape recognition. The histograms (d); (e) and (f) correspond to the parcels with the greatest mean z-score of their respective tasks.

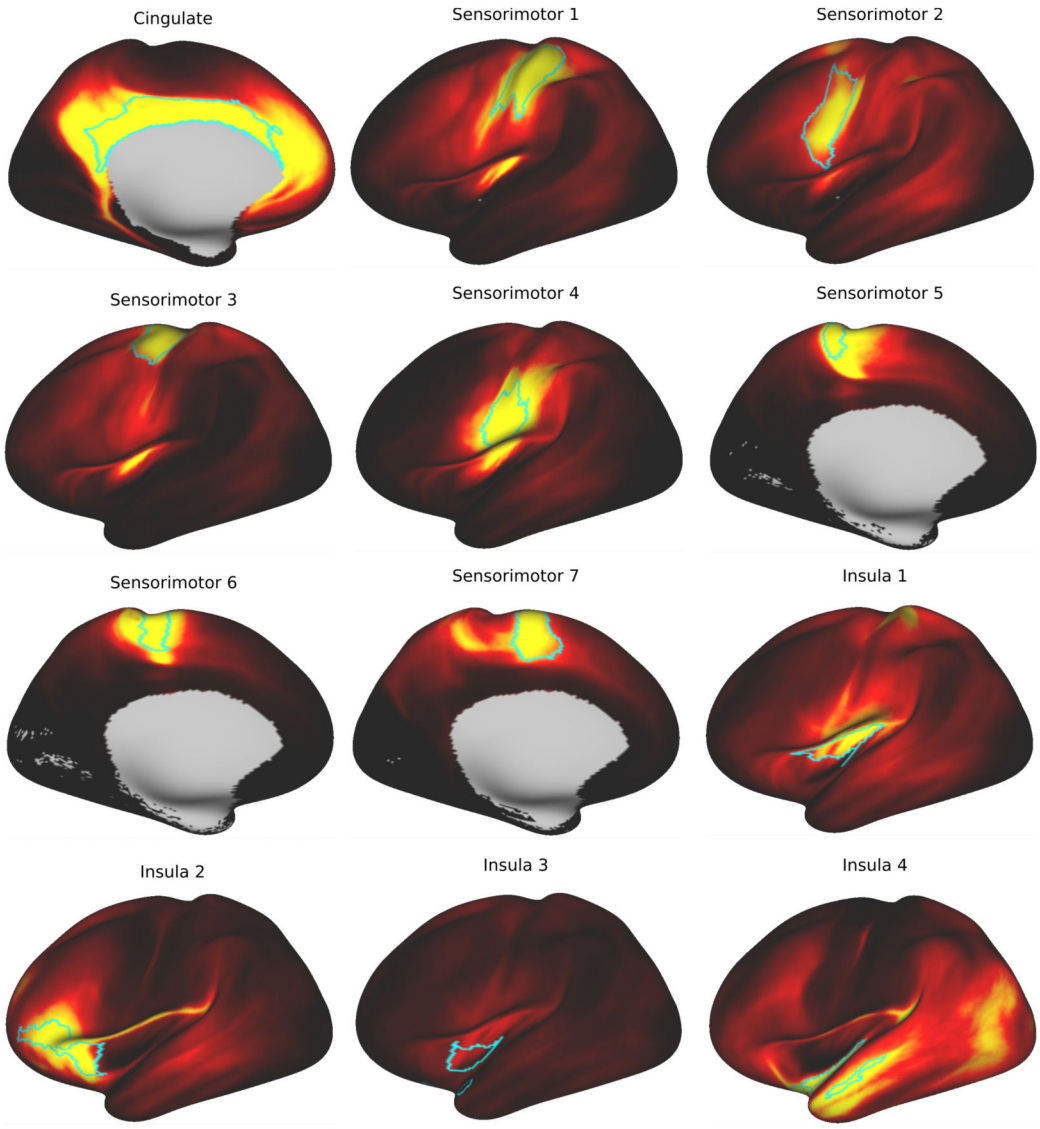

Figure 13.

Connectivity fingerprint for different parcels in our groupwise parcellation. The names in the titles are given after the anatomical structure that they subdivide (or contain, as with the Fusiform).

Table 1

Correlation value reported (Neurosynth)

Spatial correlation value reported by Neurosynth for specific terms in each parcel of Thiebaut de Schotten et al. (2016) and for our parcels. Enumeration comes from figure 6.

Parcel	Term	*r* (Thiebaut et al.)	*r* (Ours)
1	foot	0.267	**0.319**
2	motor	0.129	**0.208**
3	eye field	0.081	0.048
4	speech production	0.077	**0.138**
5	pre sma	0.245	0.234
6	phonological	0.206	0.019
7	-	-	-
8	executive control	0.049	0.042
9	-	-	-
10	semantic	0.178	**0.226**
11	social	0.137	0.110
12	semantic	0.139	0.086

Table 2

Statistics on z-score distribution in parcels from figure 9

Minimum; maximum and mean z-score contained by each of the parcels enumerated in figure 9. The highest z-score of each map is reported to facilitate comparison. T-Avg: Tongue movement versus average; RH-Avg: Right Hand Movement versus average; RF-Avg: Right Foot Movement versus average.

Contrast	Parcel	Min.	Max.	Mean ± Std. Dev.	Max. Score in Map
T-Avg	**1**	−3.62	15.03	5.67±4.91	15.03
T-Avg	**2**	4.11	14.88	10.30 ± 2.56	15.03
RH-Avg	**3**	−7.02	14.50	5.05 ± 4.95	14.50
RH-Avg	**4**	−11.25	14.07	6.35 ± 6.25	14.50
RF-Avg	**5**	−7.10	9.57	2.99 ± 3.84	14.56
RF-Avg	**6**	1.04	14.01	7.13 ± 3.20	14.56
RF-Avg	**7**	−0.83	13.98	9.23 ± 3.32	14.56
RF-Avg	**8**	−0.46	14.56	8.73 ± 3.81	14.56

Table 3

Statistics on z-score distribution in parcels from figure 10

Table 3. Minimum; maximum and mean z-score contained by each of the parcels enumerated in figure 10. The highest z-score of each map is reported to facilitate comparison. Faces-Shapes: Face recognition versus shape recognition contrast; Shapes-Faces: Shape recognition versus face recognition; Story: Short story categorization.

Contrast	Parcel	Min.	Max.	Mean ± Std. Dev.	Max. Score in map
Faces-Shapes	**1**	−4.33	9.28	3.35 ± 3.51	13.45
Faces-Shapes	**2**	−7.16	12.36	4.01 ± 4.09	13.45
Faces-Shapes	**3**	−6.07	13.45	5.16 ± 5.25	13.45
Shapes-Faces	**4**	−5.73	5.37	0.93 ± 1.78	8.79
Shapes-Faces	**5**	−4.11	7.67	1.11 ± 2.11	8.79
Shapes-Faces	**6**	−1.13	5.94	3.17 ± 1.49	8.79
Story	**7**	−3.72	12.02	6.72 ± 3.35	12.02
Story	**8**	−3.24	11.92	7.41 ± 2.50	12.02